

CHAPTER 11: COORDINATION CHEMISTRY III: ELECTRONIC SPECTRA

11.1 a. p^3 There are $(6!)/(3!3!) = 20$ microstates:

		M_S			
		-3/2	-1/2	1/2	3/2
M_L	+2		$1^+ 1^- 0^-$	$1^+ 1^- 0^+$	
	+1		$1^+ 1^- -1^-$ $1^- 0^- 0^+$	$1^+ 1^- -1^+$ $1^+ 0^- 0^+$	
	0	$1^- 0^- -1^-$	$1^+ 0^- -1^-$ $1^- 0^+ -1^-$ $1^- 0^- -1^+$	$1^+ 0^+ -1^-$ $1^+ 0^- -1^+$ $1^- 0^+ -1^+$	$1^+ 0^+ -1^+$
	-1		$-1^+ -1^- 1^-$ $-1^- 0^- 0^+$	$-1^+ -1^- 1^+$ $-1^+ 0^- 0^+$	
	-2		$-1^+ -1^- 0^-$	$-1^+ -1^- 0^+$	

Terms: $L = 0, S = 3/2$: 4S (ground state)

$L = 2, S = 1/2$: 2D

$L = 1, S = 1/2$: 2P

b. p^1d^1 There are $\frac{6!}{1!5!} \times \frac{10!}{1!9!} = 60$ microstates:

		M_S		
		-1	0	1
M_L	3	$1^- 2^-$	$1^- 2^+, 1^+ 2^-$	$1^+ 2^+$
	2	$1^- 1^-$ $0^- 2^-$	$1^+ 1^-, 1^- 1^+$ $0^- 2^+, 0^+ 2^-$	$1^+ 1^+$ $0^+ 2^+$
	1	$1^- 0^-$ $0^- 1^-$ $-1^- 2^-$	$1^+ 0^-, 0^+ 1^-$ $1^- 0^+, 0^- 1^+$ $-1^- 2^+, -1^+ 2^-$	$1^+ 0^+$ $0^+ 1^+$ $-1^+ 2^+$
	0	$1^- -1^-$ $0^- 0^-$ $-1^- 1^-$	$1^+ -1^-, 1^- -1^+$ $0^- 0^+, 0^+ 0^-$ $-1^+ 1^-, -1^- 1^+$	$1^+ -1^+$ $0^+ 0^+$ $-1^+ 1^+$
	-1	$-1^- 0^-$ $0^- -1^-$ $1^- -2^-$	$-1^+ 0^-, 0^+ -1^-$ $-1^- 0^+, 0^- -1^+$ $1^- -2^+, 1^+ -2^-$	$-1^+ 0^+$ $0^+ -1^+$ $1^+ -2^+$
	-2	$-1^- -1^-$ $0^- -2^-$	$-1^+ -1^-, -1^- -1^+$ $0^+ -2^-, 0^- -2^+$	$-1^- -1^+$ $0^+ -2^+$
	-3	$-1^- -2^-$	$-1^- -2^+, -1^+ -2^-$	$-1^+ -2^+$

Terms: $L = 3, S = 1$ 3F (ground state)

$L = 3, S = 0$ 1F

$L = 2, S = 1$ 3D

$L = 2, S = 0$ 1D

$L = 1, S = 1$ 3P

$L = 1, S = 0$ 1P

The two electrons have quantum numbers that are independent of each other, because the electrons are in different orbitals. Because they have different l values, the electrons can have the same m_l and m_s values.

11.2 For p^3 : $L = 0, S = 3/2$, the term 4S has $J = 3/2$ only ($|L+S| = |L-S|$). Therefore, the ground state is $^4S_{3/2}$.

For p^1d^1 : $L = 3, S = 1$, the term 3F has $J = 4, 3, 2$. Since both levels are less than half filled, the state having lowest J has lowest energy, and the ground state is 3F_2 .

11.3 a. s^1d^1 There are $\frac{2!}{1!1!} \times \frac{10!}{1!9!} = 20$ microstates:

M_S

	-1	0	+1
+2	$0^- 2^-$	$0^- 2^+, 0^+ 2^-$	$0^+ 2^+$
+1	$0^- 1^-$	$0^- 1^+, 0^+ 1^-$	$0^+ 1^+$
0	$0^- 0^-$	$0^- 0^+, 0^+ 0^-$	$0^+ 0^+$
-1	$0^- -1^-$	$0^- -1^+, 0^+ -1^-$	$0^+ -1^+$
-2	$0^- -2^-$	$0^- -2^+, 0^+ -2^-$	$0^+ -2^+$

b. Terms: $L = 2, S = 1$: 3D ; $L = 2, S = 0$: 1D

c. The 3D , with the higher spin multiplicity, is the lower energy term.

11.4 a. d^1f^1 There are $\frac{10!}{1!9!} \times \frac{14!}{1!13!} = 140$ microstates:

M_S

	-1	0	+1
+5	$2^- 3^-$	$2^- 3^+, 2^+ 3^-$	$2^+ 3^+$
+4	$2^- 2^-$ $1^- 3^-$	$2^- 2^+, 2^+ 2^-$ $1^- 3^+, 1^+ 3^-$	$2^+ 2^+$ $1^+ 3^+$
+3	$2^- 1^-$ $1^- 2^-$ $0^- 3^-$	$2^- 1^+, 2^+ 1^-$ $1^- 2^+, 1^+ 2^-$ $0^- 3^+, 0^+ 3^-$	$2^+ 1^+$ $1^+ 2^+$ $0^+ 3^+$
+2	$2^- 0^-$ $1^- 1^-$ $0^- 2^-$ $-1^- 3^-$	$2^- 0^+, 2^+ 0^-$ $1^- 1^+, 1^+ 1^-$ $0^- 2^+, 0^+ 2^-$ $-1^- 3^+, -1^+ 3^-$	$2^+ 0^+$ $1^+ 1^+$ $0^+ 2^+$ $-1^+ 3^+$
+1	$2^- -1^-$ $1^- 0^-$ $0^- 1^-$ $-1^- 2^-$ $-2^- 3^-$	$2^- -1^+, 2^+ -1^-$ $1^- 0^+, 1^+ 0^-$ $0^- 1^+, 0^+ 1^-$ $-1^- 2^+, -1^+ 2^-$ $-2^- 3^+, -2^+ 3^-$	$2^+ -1^+$ $1^+ 0^+$ $0^+ 1^+$ $-1^+ 2^+$ $-2^+ 3^+$
0	$2^- -2^-$ $1^- -1^-$ $0^- 0^-$ $-1^- 1^-$ $-2^- 2^-$	$2^- -2^+, 2^+ -2^-$ $1^- -1^+, 1^+ -1^-$ $0^- 0^+, 0^+ 0^-$ $-1^- 1^+, -1^+ 1^-$ $-2^- 2^+, -2^+ 2^-$	$2^+ -2^+$ $1^+ -1^+$ $0^+ 0^+$ $-1^+ 1^+$ $-2^+ 2^+$
-1	$-2^- 1^-$ $-1^- 0^-$ $0^- -1^-$ $1^- -2^-$ $2^- -3^-$	$-2^- 1^+, -2^+ 1^-$ $-1^- 0^+, -1^+ 0^-$ $0^- -1^+, 0^+ -1^-$ $1^- -2^+, 1^+ -2^-$ $2^- -3^+, 2^+ -3^-$	$-2^+ 1^+$ $-1^+ 0^+$ $0^+ -1^+$ $1^+ -2^+$ $2^+ -3^+$

continued

-2	$-2^- 0^-$ $-1^- -1^-$ $0^- -2^-$ $1^- -3^-$	$-2^- 0^+, -2^+ 0^-$ $-1^- -1^+, -1^+ -1^-$ $0^- -2^+, 0^+ -2^-$ $1^- -3^+, 1^+ -3^-$	$-2^+ 0^+$ $-1^+ -1^+$ $0^+ -2^+$ $1^+ -3^+$
-3	$-2^- -1^-$ $-1^- -2^-$ $0^- -3^-$	$-2^- -1^+, -2^+ -1^-$ $-1^- -2^+, -1^+ -2^-$ $0^- -3^+, 0^+ -3^-$	$-2^+ -1^+$ $-1^+ -2^+$ $0^+ -3^+$
-4	$-2^- -2^-$ $-1^- -3^-$	$-2^- -2^+, -2^+ -2^-$ $-1^- -3^+, -1^+ -3^-$	$-2^+ -2^+$ $-1^+ -3^+$
-5	$-2^- -3^-$	$-2^- -3^+, -2^+ -3^-$	$-2^+ -3^+$

- b. Terms: $L = 5, S = 1$: 3H ; $L = 5, S = 0$: 1H ; $L = 4, S = 1$: 3G ; $L = 4, S = 0$: 1G ;
 $L = 3, S = 1$: 3F ; $L = 3, S = 0$: 1F ; $L = 2, S = 1$: 3D ; $L = 2, S = 0$: 1D ;
 $L = 1, S = 1$: 3P ; $L = 1, S = 0$: 1P
- c. The lowest energy term is the 3H . For this term, J has the values 6, 5, and 4. Because the subshells are less than half full, the lowest value of J provides the lowest energy: 3H_4 .

- 11.5 a. From Problem 11.1a, for a p^3 configuration there are three terms: 4S , 2D , and 2P . The J values for each of these are determined below.

For 4S : $L = 0, S = 3/2$;

Because $J = L + S, L + S - 1, \dots, |L - S|$, the quantum number J can only be $3/2$ and there is a single state for 4S : ${}^4S_{3/2}$

For 2D : $L = 2, S = 1/2$.

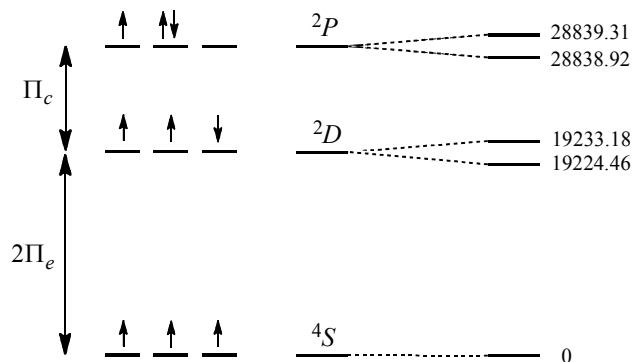
Possible J values are $5/2$ and $3/2$, and the two possible states are ${}^2D_{5/2}$ and ${}^2D_{3/2}$.

For 2P : $L = 1, S = 1/2$. Possible J values are $3/2$ and $1/2$, with states ${}^2P_{3/2}$ and ${}^2P_{1/2}$.

The lowest energy state is ${}^4S_{3/2}$ (highest multiplicity). ${}^2D_{5/2}$ and ${}^2D_{3/2}$ are next, at 19233.18 and 19224.46 cm^{-1} , and ${}^2P_{3/2}$ and ${}^2P_{1/2}$ are the highest energy at 28838.92 and 28839.31 cm^{-1} .

- b. The difference in energy between the 4S and 2D states is $2\Pi_e$. From the average of the two nearly degenerate 2D states, $\Pi_e = 9614.41 \text{ cm}^{-1}$.

The difference in energy between the averages of the 2D and 2P states is $\Pi_c = 28839.12 - 19228.82 = 9610.30 \text{ cm}^{-1}$.



- 11.6 a. $s^1 f^4$ There are $\frac{2!}{1!1!} \times \frac{14!}{1!1!3!} = 28$ microstates:

		M_S		
		-1	0	1
M_L	3	$0^- 3^-$	$0^- 3^+, 0^+ 3^-$	$0^+ 3^+$
	2	$0^- 2^-$	$0^- 2^+, 0^+ 2^-$	$0^+ 2^+$
	1	$0^- 1^-$	$0^- 1^+, 0^+ 1^-$	$0^+ 1^+$
	0	$0^- 0^-$	$0^- 0^+, 0^+ 0^-$	$0^+ 0^+$
	-1	$0^- -1^-$	$0^- -1^+, 0^+ -1^-$	$0^+ -1^+$
	-2	$0^- -2^-$	$0^- -2^+, 0^+ -2^-$	$0^+ -2^+$
	-3	$0^- -3^-$	$0^- -3^+, 0^+ -3^-$	$0^+ -3^+$

- b. Terms: $L = 3, S = 1$ 3F (ground state)
 $L = 3, S = 0$ 1F
- c. The 3F term, with the higher spin multiplicity, has the lower energy. This term has $J = 2, 3, 4$; the lowest energy term, including J , is 3F_2 .
- 11.7 a. 2D has $L = 2$ and $S = 1/2$, so $M_L = -2, -1, 0, 1, 2$ and $M_S = -1/2, 1/2$
- b. 3G has $L = 4$ and $S = 1$, so $M_L = -4, -3, -2, -1, 0, 1, 2, 3, 4$ and $M_S = -1, 0, 1$
- c. 4F has $L = 3$ and $S = 3/2$, so $M_L = -3, -2, -1, 0, 1, 2, 3$ and $M_S = -3/2, -1/2, 1/2, 3/2$
- 11.8 a. 2D with $J = 5/2, 3/2$ fits an excited state of $d^3, {}^2D_{3/2}$
- b. 3G with $J = 5, 4, 3$ fits an excited state of $d^4, {}^3G_3$
- c. 4F with $J = 9/2, 7/2, 5/2, 3/2$ fits the ground state of $d^7, {}^4F_{9/2}$
- 11.9 $\epsilon = 0.038 \frac{\text{L}}{\text{mol cm}}$ $A = 0.10$ $l = 1.00 \text{ cm}$
 $A = \epsilon lc; c = \frac{A}{\epsilon l} = \frac{0.10}{\left(0.038 \frac{\text{L}}{\text{mol cm}}\right)(1.00 \text{ cm})} = 2.6 \frac{\text{mol}}{\text{L}}$
- 11.10 a. $\bar{\nu} = 24,900 \text{ cm}^{-1}$
 $\lambda = \frac{1}{\bar{\nu}} = \frac{1}{24,900 \text{ cm}^{-1}} = 4.02 \times 10^{-5} \text{ cm} = 402 \text{ nm}$

$$\nu = \frac{c}{\lambda} = \frac{(2.998 \times 10^8 \text{ m s}^{-1})(100 \text{ cm m}^{-1})}{4.02 \times 10^{-5} \text{ cm}} = 7.46 \times 10^{14} \text{ s}^{-1}$$

b. $\lambda = 366 \text{ nm}$

$$\nu = \frac{c}{\lambda} = \frac{(2.998 \times 10^8 \text{ m s}^{-1})(10^9 \text{ nm m}^{-1})}{366 \text{ nm}} = 8.19 \times 10^{14} \text{ s}^{-1}$$

$$E = h\nu = (6.626 \times 10^{-34} \text{ Js})(8.19 \times 10^{14} \text{ s}^{-1}) = 5.43 \times 10^{-19} \text{ J}$$

11.11 J values are included in these answers:

a. $d^8 O_h M_S = 1 = S$ Spin multiplicity = $2 + 1 = 3$
 Max $M_L = 2+2+1+1+0+0-1-2 = 3 = L$, so F term. $J = 4, 3, 2$ 3F_4

b. $d^5 O_h$ high spin $M_S = 5/2 = S$ Spin multiplicity = $5 + 1 = 6$
 Max $M_L = 2+1+0-1-2 = 0 = L$, so S term. $J = 5/2$ ${}^6S_{5/2}$

$d^5 O_h$ low spin $M_S = 1/2 = S$ Spin multiplicity = $1 + 1 = 2$
 Max $M_L = 2+2+1+1+0 = 6 = L$, so I term. $J = |L \pm S| = 11/2, 13/2$ ${}^2I_{11/2}, {}^2I_{13/2}$
 (J is uncertain in this case; the usual rule does not apply because the level is exactly half full)

c. $d^4 T_d M_S = 2 = S$ Spin multiplicity = $4 + 1 = 5$
 Max $M_L = 2+1+0-1 = 2 = L$, so D term. $J = 4, 3, 2, 1, 0$ 5D_0

d. $d^9 D_{4h} M_S = 1/2 = S$ Spin multiplicity = $1+1=2$
 Max $M_L = 2+2+1+1+0+0-1-1-2 = 2 = L$, so D term. $J = |L \pm S| = 5/2, 3/2$ ${}^2D_{5/2}$

11.12 a. $[M(\text{H}_2\text{O})_6]^{2+}$ There are two possibilities, $M = \text{Ni} (d^8)$ and $M = \text{Ti} (d^2)$. The complex $[\text{Ni}(\text{H}_2\text{O})_6]^{2+}$ is well known. However, titanium strongly prefers the 3+ oxidation state, and $[\text{Ti}(\text{H}_2\text{O})_6]^{2+}$ has not been well characterized. A third possibility would be low spin $[\text{Cr}(\text{H}_2\text{O})_6]^{2+}$ —if this complex were low spin. However, stronger field ligands than H_2O are necessary for complexes of $\text{Cr}(\text{II})$ to be low spin.

b. $[M(\text{NH}_3)_6]^{3+}$ There are several possibilities, for $M = \text{Ti} (d^1)$, $\text{V} (d^2)$, $\text{Cr} (d^3)$, and $\text{Co} (d^6)$, among first row transition metals that commonly exhibit a 3+ oxidation state.

Excitation of the single d electron from the t_{2g} to e_g levels in $[\text{Ti}(\text{NH}_3)_6]^{3+}$ leads to asymmetric occupation of the e_g , a configuration susceptible to Jahn-Teller distortion (Section 10.5). Like $[\text{Ti}(\text{H}_2\text{O})_6]^{3+}$ (Figure 11.8), $[\text{Ti}(\text{NH}_3)_6]^{3+}$ shows splitting of its absorption band (excitation from ${}^2T_{2g}$ to 2E_g (Figure 11.11)).

Similarly, in $[\text{V}(\text{NH}_3)_6]^{3+}$, excitation of an electron from t_{2g} to e_g would give asymmetric occupation of the e_g , a configuration that could potentially give rise to distortion and splitting of absorption bands. However, spectra of d^3 octahedral complexes typically do not show such splitting (see spectrum of $[\text{V}(\text{H}_2\text{O})_6]^{3+}$ in Figure 11.8), but have broad overlapping bands that dominate the visible spectra.

Excitation of a t_{2g} electron to an e_g level in the d^3 complex $[\text{Cr}(\text{NH}_3)_6]^{3+}$ leads to asymmetric occupation of the e_g , potentially giving rise to band splitting in the absorption spectrum.

The low-spin d^6 complex $[\text{Co}(\text{NH}_3)_6]^{3+}$ does show splitting consistent with distortion of the excited state resulting from excitation of a t_{2g} electron to the previously empty e_g level. Such splitting is also observed in the d^6 iron (II) complex $[\text{Fe}(\text{H}_2\text{O})_6]^{2+}$ (Figure 11.8).

The last three transition metals in this row, Ni, Cu, and Zn, do not exhibit stable 3+ complexes of formula $[\text{M}(\text{NH}_3)_6]^{3+}$. Comparable complexes for Mn and Fe have not been well characterized.

- c. $[\text{M}(\text{H}_2\text{O})_6]^{2+}$ If $\text{M} = \text{Zn}$, all t_{2g} and e_g orbitals are filled, and consequently no $d-d$ transitions are possible. As a consequence, the d^{10} complex $[\text{Zn}(\text{H}_2\text{O})_6]^{2+}$ is colorless. The d^5 complex $[\text{Mn}(\text{H}_2\text{O})_6]^{2+}$ is nearly colorless (*very* pale pink) because it has no excited state of the same spin multiplicity (6) as the ground state (see Tanabe-Sugano diagram in Figure 11.7). The electronic spectrum (Figure 11.8) shows absorption bands approximately two orders of magnitude smaller than for other first row $[\text{M}(\text{H}_2\text{O})_6]^{2+}$ complexes.

11.13 $[\text{Ni}(\text{H}_2\text{O})_6]^{2+}$ For d^8 ions, the energy of the lowest energy band is Δ_o , so $\Delta_o = 8,700 \text{ cm}^{-1}$. The bands are split due to Jahn-Teller distortion in the excited state.

11.14 a. $[\text{Cr}(\text{C}_2\text{O}_4)_3]^{3-}$ is Cr(III), d^3 . Δ_o is equal to the lowest energy band, so $\Delta_o = 17,400 \text{ cm}^{-1}$.

b. $[\text{Ti}(\text{NCS})_6]^{3-}$ is Ti(III), d^1 . Δ_o is the energy of the single band; $\Delta_o = 18,400 \text{ cm}^{-1}$. The band is split due to Jahn-Teller distortion of the excited state.

c. $[\text{Ni}(\text{en})_3]^{2+}$ is Ni(II), d^8 . The lowest energy band corresponds to Δ_o ; $\Delta_o = 11,200 \text{ cm}^{-1}$.

d. $[\text{VF}_6]^{3-}$ is V(III), d^2 . Following the example on pp. 427 - 428, we find the ratio ν_2/ν_1 and then Δ_o/B : $\nu_2/\nu_1 = 1.57$ at $\Delta_o/B = 26$. From the Tanabe-Sugano diagram at $\Delta_o/B = 26$,

$$\begin{array}{lll} \nu_1: E/B = 24.1 & E = 24.1 B = 14,800 \text{ cm}^{-1} & B = 614 \text{ cm}^{-1} \\ \nu_2: E/B = 37.0 & E = 37.0 B = 23,250 \text{ cm}^{-1} & B = 628 \text{ cm}^{-1} \end{array}$$

Average $B = 621 \text{ cm}^{-1}$, $\Delta_o = 26 B = 16,100 \text{ cm}^{-1}$ (On the basis of the data in this and following problems, the values of B and Δ_o should be rounded to two significant digits; additional digits are shown here to assist in checking calculations.)

e. V(III) is a d^2 ion. Again following the example on pp. 427 - 428, $\nu_2 = 21,413 \text{ cm}^{-1}$ and $\nu_1 = 14,409 \text{ cm}^{-1}$, $\nu_2/\nu_1 = 1.49$. From the Tanabe-Sugano diagram at $\Delta_o/B = 34.5$,

$$\begin{array}{lll} \nu_1: E/B = 29 & E = 29 B = 14,409 \text{ cm}^{-1} & B = 497 \text{ cm}^{-1} \\ \nu_2: E/B = 44 & E = 44 B = 21,413 \text{ cm}^{-1} & B = 487 \text{ cm}^{-1} \end{array}$$

Average $B = 492 \text{ cm}^{-1}$, $\Delta_o = 34.5 B = 16,970 \text{ cm}^{-1}$

11.15 $[\text{Co}(\text{NH}_3)_6]^{2+}$, d^7 . As in Problem 11.14d:

$\nu_2/\nu_1 = 2.34$ at $\Delta_o/B = 11$. From the Tanabe-Sugano diagram at $\Delta_o/B = 11$,

$$\begin{array}{lll} \nu_1: E/B = 10 & E = 10 B = 9,000 \text{ cm}^{-1} & B = 900 \text{ cm}^{-1} \\ \nu_2: E/B = 22.5 & E = 22.5 B = 21,100 \text{ cm}^{-1} & B = 938 \text{ cm}^{-1} \end{array}$$

Average $B = 919 \text{ cm}^{-1}$, $\Delta_o = 11 B = 10,100 \text{ cm}^{-1}$

- 11.16** a. $t_{2g}^4 e_g^2$ The t_{2g} level is a triply degenerate asymmetrically occupied state, so it is T .
- b. t_{2g}^6 This is a nondegenerate state, completely occupied, so it is A .
- c. $t_{2g}^3 e_g^3$ This is an excited state, with the t_{2g} level uniformly occupied and the e_g level doubly degenerate, so it is E .
- d. t_{2g}^5 This is a triply degenerate state, T . (Vacancies in the orbitals can be treated similarly to electrons.)
- e. e_g Another excited state, this is doubly degenerate, E .
- 11.17** The complexes with potential degeneracies are those with d^1 , d^2 , d^4 , d^7 and d^9 , low-spin d^5 , and high-spin d^6 configurations. The strongest effects are with high-spin d^4 , low-spin d^7 , and d^9 complexes, corresponding to $[\text{Mn}(\text{NH}_3)_6]^{3+}$, $[\text{Ni}(\text{NH}_3)_6]^{3+}$, and the unknown $[\text{Zn}(\text{NH}_3)_6]^{3+}$. Weaker effects might be seen with $[\text{Ti}(\text{NH}_3)_6]^{3+}$, $[\text{V}(\text{NH}_3)_6]^{3+}$, low-spin $[\text{Fe}(\text{NH}_3)_6]^{3+}$, and high-spin $[\text{Co}(\text{NH}_3)_6]^{3+}$, all of which are unknown or unstable. Other ligands are needed to stabilize ions containing these 3+ metal ions.
- 11.18** The $5d$ orbitals of Re are higher in energy than the $3d$ orbitals of Mn, so an LMCT excitation requires more energy for ReO_4^- . In addition, since the molecular orbitals derived primarily from the $3d$ orbitals of MnO_4^- are lower in energy than the corresponding MO's of ReO_4^- , MnO_4^- is better able to accept electrons; it is a better oxidizing agent.
- 11.19** The order of energy of the charge transfer bands is $\text{I} < \text{Br} < \text{Cl}$. LMCT in low-spin d^6 $[\text{Co}(\text{NH}_3)_5\text{X}]^{2+}$ can be approximated (since this complex does not have O_h symmetry) as excitation into the LUMO (empty e_g orbitals of high z^2 and $x^2 - y^2$ character) from lower energy, relatively nonbonding (or weakly bonding π -donor) orbitals with high halide valence orbital character. It is reasonable to approximate the LUMO energies as very similar for this series of Co(III) cations. However, the lower-energy orbitals with high halide valence orbital character will be lowest for the most electronegative chloride, and highest for the least electronegative iodide. This difference results in $[\text{Co}(\text{NH}_3)_5\text{I}]^{2+}$ having the lowest-energy predicted LMCT band. From an HSAB perspective, iodide is softer and can lose an electron most easily in an LMCT process.
- 11.20** Comparing $[\text{Fe}(\text{CN})_6]^{3-}$ (low spin d^5) and $[\text{Fe}(\text{CN})_6]^{4-}$ (low spin d^6), where CN^- is a σ donor and a π acceptor: the t_{2g} orbitals of $[\text{Fe}(\text{CN})_6]^{3-}$ contain 5 electrons, allowing LMCT from the ligand orbitals to either t_{2g} or e_g levels. The t_{2g} levels of $[\text{Fe}(\text{CN})_6]^{4-}$ are full, so only the higher e_g levels are available for LMCT. MLCT transitions ($t_{2g} \rightarrow \pi^*$) are also possible for either complex.
- 11.21** a. O^{2-} and Cl^- are both σ and π donors, and the metal ions are Cr(V) and Mo(V) (the ligands are Cl^- and O^{2-}). Metal d orbitals, influence of Cl^- ligands:

	e_σ	e_π	Total
z^2	2	0	$2e_\sigma$
$x^2 - y^2$	3	0	$3e_\sigma$
xy	0	4	$4e_\pi$
xz	0	3	$3e_\pi$
yz	0	3	$3e_\pi$

Metal d orbitals, influence of O^{2-} ligands:

	e_σ	e_π	Total
z^2	1	0	e_σ
$x^2 - y^2$	0	0	0
xy	0	0	0
xz	0	1	e_π
yz	0	1	e_π

C_{4v}	E	$2C_4$	C_2	$2\sigma_v$	$2\sigma_d$	
A_1	1	1	1	1	1	z^2
B_1	1	-1	1	1	-1	$x^2 - y^2$
B_2	1	-1	1	-1	1	xy
E	2	0	-2	0	0	(xz, yz)

Overall, from lower energy (top) to higher energy (bottom), the d orbital energies are:

$$\begin{array}{ll}
 xy & 4e_\pi(\text{Cl}) \\
 xz \text{ and } yz & 3e_\pi(\text{Cl}) + e_\pi(\text{O}) \\
 z^2 & 2e_\sigma(\text{Cl}) + e_\sigma(\text{O}) \\
 x^2 - y^2 & 3e_\sigma(\text{Cl})
 \end{array}$$

- b. The symmetry labels of the orbitals are given in the C_{4v} character table.
- c. The lowest d orbital has an energy of $2e_\pi(\text{Cl})$; the next have energies of $2e_\pi(\text{Cl}) + e_\pi(\text{O})$. Because these are d^1 complexes, the transitions given provide the HOMO/LUMO gaps in these complexes. The interactions between metal and ligand are generally stronger for a second row transition metal than for the first row, raising the LUMO energy in the Mo case. It is reasonable to expect the larger Mo(V) to offer better π overlap with the ligand donor orbitals relative to the smaller Cr(V).

11.22 $[\text{V}(\text{CO})_6]^- < \text{Cr}(\text{CO})_6 < [\text{Mn}(\text{CO})_6]^+$ As the nuclear charge on the metal increases, the metal orbitals are drawn to lower energies. Consequently, the MLCT bands should increase in energy.

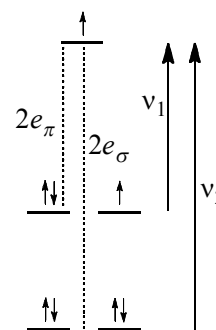
11.23 a. At 80K: $\mu_S = 0.65 = \sqrt{n(n+2)}$ $n = 0.19$
 At 300K: $\mu_S = 5.2 = \sqrt{n(n+2)}$ $n = 4.3$

- b. The complex is near the low-spin – high-spin boundary of the d^6 Tanabe-Sugano diagram. High spin becomes increasingly favored as the temperature increases.

11.24 a. ML_2 , using positions 1 and 6, with O^{2-} both a σ and π donor:

	e_σ	e_π	Total
z^2	2	0	$2e_\sigma$
$x^2 - y^2$	0	0	0
xy	0	0	0
xz	0	2	$2e_\pi$
yz	0	2	$2e_\pi$

- b. If this is a high-spin complex, there are 4 electrons in the lowest levels ($xy, x^2 - y^2$), 3 in the next two (xz, yz), and 1 in the highest (z^2). Electronic transitions can be either from the middle levels to the top, and from the bottom levels to the middle and the top—three possibilities in all. According to the reference, the transitions seen are from the middle and the bottom levels to the top level.



- c. Assigning the transitions as in part b:

$$E = 2e_{\sigma} = 16,000 \text{ cm}^{-1} \quad E = 2e_{\pi} = 9,000 \text{ cm}^{-1}$$

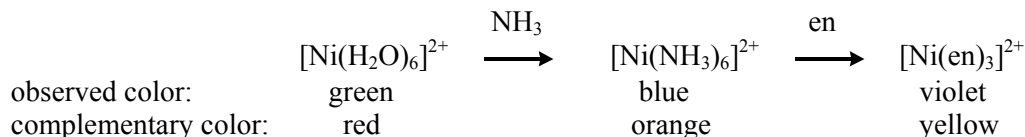
$$\text{so } e_{\sigma} = 8,000 \text{ cm}^{-1} \text{ and } e_{\pi} = 4,500 \text{ cm}^{-1}$$

The reference provides a much more detailed analysis, including a discussion of the paramagnetism of this complex and other factors related to its electronic spectrum.

11.25	$\text{Re}(\text{CO})_3(\text{P}(\text{OPh}_3))(\text{DBSQ})$	$18,250 \text{ cm}^{-1}$
	$\text{Re}(\text{CO})_3(\text{PPh}_3)(\text{DBSQ})$	$17,300 \text{ cm}^{-1}$
	$\text{Re}(\text{CO})_3(\text{NEt}_3)(\text{DBSQ})$	$16,670 \text{ cm}^{-1}$

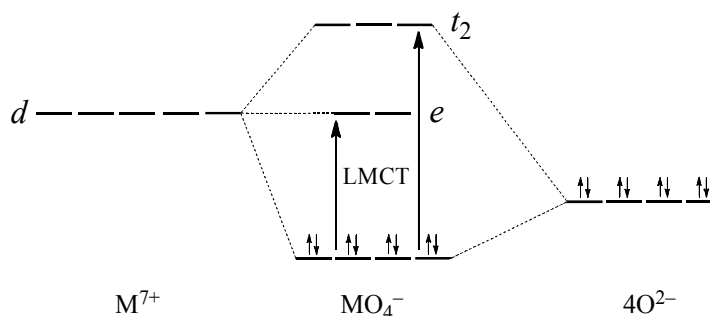
NEt_3 is the strongest donor ligand in this series. Therefore, the metal in the complex $\text{Re}(\text{CO})_3(\text{NEt}_3)(\text{DBSQ})$ has the greatest concentration of electrons and the greatest tendency for electron transfer to acceptor orbitals. Since this complex also has the lowest-energy charge transfer band, we may assign this as MLCT.

- 11.26 a. RuO_4^{2-} has the highest value of Δ_t . Δ_t increases with the oxidation state of the metal and in general is greater for second row than for first row metals. The overall trend is $\text{RuO}_4^{2-} > \text{FeO}_4^{2-} > \text{MnO}_4^{3-} > \text{CrO}_4^{4-}$.
- b. The nuclear charge of iron is greatest in this isoelectronic series and exerts the strongest attraction for bonding electrons. As a result, FeO_4^{2-} has the shortest metal-oxygen distance, 165 pm, in comparison with 170 pm for MnO_4^{3-} and 176 pm for CrO_4^{4-} and RuO_4^{2-} .
- c. As the nuclear charge of the metal increases, the metal orbitals' energies are decreased (further stabilized). Consequently, less energy is needed to excite electrons from ligand orbitals to these metal orbitals. These are LMCT absorptions.
- 11.27 Aqueous solutions of $\text{Ni}(\text{NO}_3)_2$ contain the green $[\text{Ni}(\text{H}_2\text{O})_6]^{2+}$ ion; nitrate is the counterion. Addition of aqueous NH_3 replaces the H_2O ligands in $[\text{Ni}(\text{H}_2\text{O})_6]^{2+}$ to give blue $[\text{Ni}(\text{NH}_3)_6]^{2+}$. As a bidentate ligand, en can replace two NH_3 ligands; three en ligands can therefore replace all six NH_3 ligands to form violet $[\text{Ni}(\text{en})_3]^{2+}$:



The complementary colors in this series have increasing energies, indicating that en has the strongest effect on Δ_o , and H_2O has the weakest effect. This is consistent with the positions of these ligands in the spectrochemical series.

- 11.28 a. These colors are most likely the consequence of LMCT transitions, from orbitals that are primarily from the oxide ligands to orbitals that are primarily from the metal:



- b. In TcO_4^- , the separation between the donor orbitals of the O^{2-} ligands and the acceptor orbitals is greater than in MnO_4^- . As a consequence, TcO_4^- absorbs light of higher energy (green) than MnO_4^- (yellow). Actually, most of the absorption by TcO_4^- is in the ultraviolet, with the pale red color a result of a tail of the absorption band extending into the visible.
- c. The metal-ligand interactions in MnO_4^{2-} (Mn(VI)) are weaker than in MnO_4^- (Mn(VII)), and the separation of donor and acceptor orbitals in MnO_4^{2-} is smaller, meaning that less energy (red light) is necessary for excitation than in MnO_4^- (yellow). Also worth noting: the Mn—O bond distance is longer in MnO_4^{2-} (165.9 pm) than in MnO_4^- (162.9 pm), an indication of weaker bonding in the former.
- 11.29 a. At 350 nm:

$$\epsilon = \frac{A}{lc} = \frac{2.34}{(1.00\text{cm})(2.00 \times 10^{-4}\text{M})}$$

$$= 11,700 \text{ L mol}^{-1} \text{ cm}^{-1}$$
- At 514 nm:

$$\epsilon = \frac{A}{lc} = \frac{0.532}{(1.00\text{cm})(2.00 \times 10^{-4}\text{M})}$$

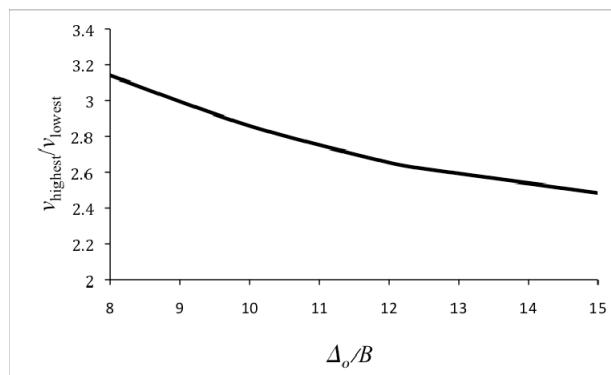
$$= 2,660 \text{ L mol}^{-1} \text{ cm}^{-1}$$
- At 590 nm:

$$\epsilon = \frac{A}{lc} = \frac{0.370}{(1.00\text{cm})(2.00 \times 10^{-4}\text{M})}$$

$$= 1,850 \text{ L mol}^{-1} \text{ cm}^{-1}$$
- At 1540 nm:

$$\epsilon = \frac{A}{lc} = \frac{0.0016}{(1.00\text{cm})(2.00 \times 10^{-4}\text{M})}$$

$$= 8.0 \text{ L mol}^{-1} \text{ cm}^{-1}$$
- b. Because of their high intensity, the bands at 350, 514, and 590 nm are probably charge transfer bands. However, the low molar absorptivity of the band at 1540 nm indicates that it is probably a $d-d$ transition (see examples in Figure 11.8).
- 11.30 These are all d^8 complexes, with three excited states of the same spin multiplicity as the ground state. For d^8 , Δ_o = energy of the lowest energy band. B can be calculated by using the method of Problem 11.14. Δ_o is the difference between the transitions ${}^3A_2 \rightarrow {}^3T_1$ and ${}^3A_2 \rightarrow {}^3T_2$; a graph of ν_2/ν_1 versus Δ_o/B needs to be prepared for $d^8 \text{ Ni}^{2+}$ in order to calculate B , as described on pages 427 - 428. A plot of the ratio of the highest energy band to the lowest energy band is shown on the next page.



Species	Ratio	Δ_o/B	$\Delta_o(\text{cm}^{-1})$	$B(\text{cm}^{-1})$
$[\text{Ni}(\text{H}_2\text{O})_6]^{2+}$	3.06	8.8	8500	970
$[\text{Ni}(\text{NH}_3)_6]^{2+}$	2.62	12.5	10500	840
$[\text{Ni}(\text{OS}(\text{CH}_3)_2)_6]^{2+}$	3.11	8.4	7728	920
$[\text{Ni}(\text{dma})_6]^{2+}$	3.14	8.0	7576	950

11.31 a. These are both high-spin d^7 complexes, for which the ground-state term symbol is 4F (see Figure 11.7)

b. There are three possible transitions, all originating from the $^4T_1(^4F)$ and going to the 4T_2 , 4A_2 , and $^4T_1(^4P)$ levels.

c. For $[\text{Co}(\text{bipy})_3]^{2+}$, the ratio $\frac{\nu_2}{\nu_1} = \frac{22,000 \text{ cm}^{-1}}{11,300 \text{ cm}^{-1}} = 1.95$. From Figure 11.14, this comes at $\frac{\Delta_o}{B} = 17$, at which:

$$\text{for the } 22,000 \text{ cm}^{-1} \text{ band: } \frac{E}{B} = 28 \text{ and } B = \frac{22,000 \text{ cm}^{-1}}{28} = 786 \text{ cm}^{-1}$$

$$\text{for the } 11,300 \text{ cm}^{-1} \text{ band: } \frac{E}{B} = 15 \text{ and } B = \frac{11,300 \text{ cm}^{-1}}{15} = 754 \text{ cm}^{-1}$$

$$\text{Average } B = 770 \text{ cm}^{-1}; \frac{\Delta_o}{B} = 17; \Delta_o = 13,100 \text{ cm}^{-1}$$

$$\text{For a } d^7 \text{ complex, LFSE} = -\frac{4}{5} \Delta_o = -10,500 \text{ cm}^{-1}$$

$$\Delta_o \text{ for } [\text{Co}(\text{NH}_3)_6]^{2+} \text{ was calculated in Problem 11.15; } \Delta_o = 10,100 \text{ cm}^{-1}.$$

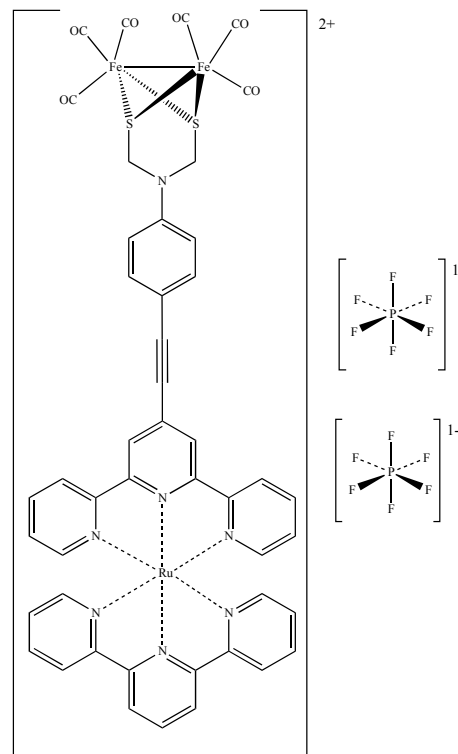
$$\text{For this } d^7 \text{ complex, LFSE} = -\frac{4}{5} \Delta_o = -8,080 \text{ cm}^{-1}$$

d. These bands should be broad (see Figure 11.8).

e. The molecular orbital energy level diagrams should be similar to Figure 10.5, with 6 electrons in t_{2g} orbitals and 1 electron in an e_g level in each case. The separation between t_{2g} and e_g orbitals should be larger in the bipy complex.

11.32 These absorption bands correspond to LMCT transitions. As the nuclear charge increases ($\text{Fe} \longrightarrow \text{Ni}$), the acceptor (largely d) orbitals decrease in energy, enabling the charge transfer transitions to occur at lower energy in the nickel complex.

11.33 The target complex structure is at right. The conjugated phenylacetylene linker is first and foremost a conjugated system to allow electronic communication between the separated metal fragments; the linker is to permit the delocalization of the $[\text{Ru}(\text{terpy})_2]^{2+}$ MLCT excited state towards the iron atoms. The reference mentions literature precedence for the effectiveness of phenylacetylene linkers in increasing covalently attached $[\text{Ru}(\text{terpy})_2]^{2+}$ excited state lifetimes, advantageous to facilitate effective transfer to the iron-sulfur fragment. The rigidity of the linker permits precise control over the distance between the Fe and Ru centers, another way to modulate the effectiveness of the electronic communication between these metal centers. Finally, from a practical standpoint, the acetylene substituent in an intermediate serves as a convenient functional group in the multi-step synthesis of the complex sketched. The most intense bands in the provided spectrum are assigned to $\pi \rightarrow \pi^*$ intraligand transitions of terpyridine



(310 nm) and MLCT of the covalently attached $[\text{Ru}(\text{terpy})_2]^{2+}$ fragment (500 nm). The complex above is unable to induce proton reduction since the intramolecular electron transfer from the $[\text{Ru}(\text{terpy})_2]^{2+}$ excited state (via MLCT) to the iron-sulfur fragment is not thermodynamically favorable. The authors speculate on various strategies to render this electron transfer favorable, including substitution of the carbon monoxide molecules with different ligands.

11.34 The excellent electron withdrawing ability of the imide function is hypothesized to stabilize the resulting reduced dithiolate diiron complex upon electron transfer from the photogenerated zinc porphyrin excited state. This proposed stabilization is expected to render the electron transfer from the zinc photosensitizer more thermodynamically favorable. The well-established utility of the imide functional group for the coupling reactions necessary to synthesize the complex is also advantageous.

The lack of ground state electronic interaction between the naphthalene monoimide (NMI) dithiolate-tethered zinc porphyrin and the iron centers was inferred by infrared spectroscopy. The infrared spectrum in the carbonyl region of the NMI dithiolate diiron complex is essentially unchanged upon covalent attachment of the zinc porphyrin. The presence of this zinc substituent has an insignificant impact on the electron density at the iron centers.